

## STRESS TRANSFERRING MECHANISMS OF COMPOSITE CES BEAM-COLUMN JOINTS SUBJECTED TO SEISMIC LOADING

Tomoya MATSUI<sup>1</sup> and Hiroshi KURAMOTO<sup>2</sup>

<sup>1</sup> Assistant Prof., Dept. of Architecture and Civil Eng., Toyohashi University of Technology, Toyohashi, Japan

<sup>2</sup> Prof., Div. of Global Architecture, Graduate School of Eng., Osaka University, Suita, Japan  
Email: matsui@tutrp.tut.ac.jp, kuramoto@arch.eng.osaka-u.ac.jp

### ABSTRACT:

In this study, three dimensional non-linear FEM analysis of beam-column joints for composite CES structural systems is conducted to verify applicability of the analysis method and modeling, together with examining the stress transferring mechanism for CES beam-column joints. The analytical results show good agreement with the experimental ones on the story shear versus story drift response for the CES joints, namely it is found that the behavior of the CES beam-column joints can be approximately simulated by the analytical method. It is confirmed that analyzed shear force in the outer concrete without steel in the joint panel region are contributed as almost the same level as those in the inner concrete surrounded by the steel flange of the beams and columns at the maximum capacity of the CES beam-column joint. It is also shown that the ultimate shear strength of the CES beam-column joints can be evaluated by a method based on the AIJ design standard for SRC structures.

**KEYWORDS:** Composite CES structure, beam-column joints, FRC, FEM analysis, Shear strength evaluation

### 1. INTRODUCTION

Steel Reinforced Concrete (SRC) Structures developed in Japan have good structural performance for resisting lateral forces imposed by wind and earthquakes, and have been adopted for medium-rise, high-rise and super high-rise buildings. However, the construction number of SRC structures has decreased since the 1990s. One of causes for decrease in the number seems to be remarkable development of new structural systems such as the high-strength reinforced concrete (RC) structures and Concrete-Filled Steel Tube (CFT) structures, but the main reason of the decrease is the construction problems in SRC structural system itself that increase construction costs and lengthen construction schedules. Even so, it could be important that SRC structures provide better seismic performance in comparison to other structural systems. Then, the authors started to develop a new composite structural system with the same or better seismic performance and workability than SRC structures, and have conducted continuing development studies on composite Concrete Encased Steel (CES) structures consisting of steel and fiber reinforced concrete (FRC).

In experimental studies on CES columns and CES beam-column joints, it was confirmed that the use of FRC made damages due to cracking and crushing of concrete reduce even under large drift angles, and the restoring force characteristics of the CES members were almost the same as that of SRC members. An evaluation method of the structural performance for CES structures is required to make CES structures practical in the future. In this paper, a three-dimensional non-linear FEM analysis of CES beam-column joints was carried out to clarify the stress transfer mechanisms of the joints. In addition, an evaluation method of the ultimate joint shear strength of CES beam-column joints is discussed.

### 2. OUTLINE OF CES BEAM-COLUMN JOINTS TEST

A total of for CES beam-column joint specimens were tested including two interior ones, Specimens CESJ-A and CESJ-B, and two exterior ones, Specimen CESJ-AE and CESJ-BE of which the scale was about 1/2.7. The dimensions and cross-section of the specimens are shown in Table 1 and Fig. 1. The specimens were set in the loading apparatus with pin supports at the ends of beams and columns as shown in Fig. 2. The column had 400

Table 1 Details of specimens

Specimen	CESJ-A	CESJ-B	CESJ-AE	CESJ-BE	
shear capacity magnification factor	1.10	0.51	2.04	0.77	
Concrete	FRC ( $F_c=30\text{MPa}$ )				
Concrete strength (MPa)	33.3	31.6	38.4	40.0	
Panel zone	Steel	H-300×220×10×15	H-300×220×4.5×15	H-300×220×10×15	H-300×220×4.5×15
column	Steel	H-300×220×10×15			
	Length:h(mm)	1300			
	$B \times D$ (mm)	400×400			
beam	Steel	H-300×150×6.5×9	H-300×200×9×19	H-300×150×6.5×9	H-300×200×9×19
	Length:l(mm)	2250			
	$B \times D$ (mm)	300×400			

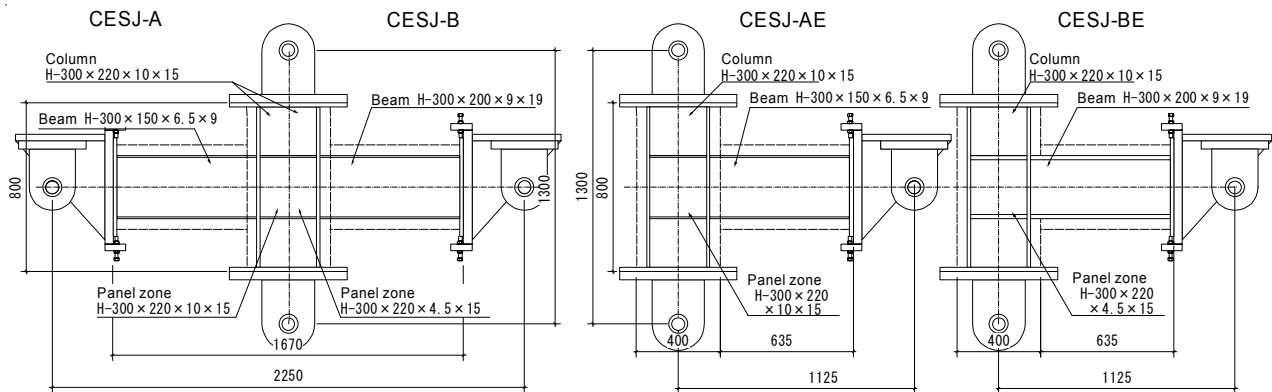


Figure 1 Test Specimens

mm square section with the height of 1,300 mm between the pin supports, while the beam had the section of 400 mm x 300 mm with the span of 2,250 mm.

The variable investigated was the shear capacity magnification factor defined as the ratio of the ultimate joint shear strength to the ultimate flexural strength of beams, where each strength is converted into the column shear. The ultimate flexural strengths of the beam and column are calculated using the generalized superposition strength theory, and ultimate shear strengths of the joints are calculated based on the AIJ design standard for SRC Structures [1] considering the absence of reinforcing bars. The shear capacity magnification factors were 1.10 for Specimen CESJ-A, 0.51 for Specimen CESJ-B, 2.04 for Specimen CESJ-AE and 0.77 for Specimen CESJ-BE, respectively. Formulas to calculate the shear strength of the joint provided in the AIJ design standard are as follows.

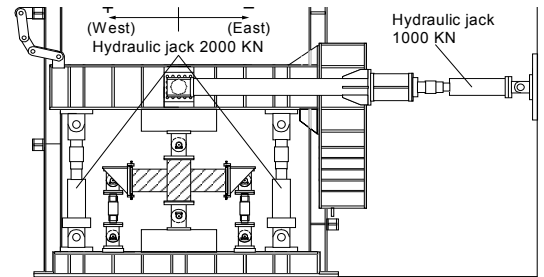


Figure 2 Loading apparatus

$${}_c Q_p = \frac{j_b \cdot l}{(l - j_c) \cdot h - j_b \cdot l} \cdot Q_p \quad (1)$$

$$Q_p = {}_J F_s \cdot {}_J \delta_c \cdot A_e + \frac{1.2 \cdot \sigma_{y_{sw}} \cdot A}{\sqrt{3}} \quad (2)$$

$${}_J F_s = \min \left( 0.12 F_c, 1.8 + \frac{3.6 F_c}{100} \right) \quad (3)$$

Where,  $Q_p$ : ultimate shear strength of joint,  ${}_c Q_p$ : shear force of column corresponding to  $Q_p$ ,  ${}_J F_s$ : shear strength of concrete,  $F_c$ : compressive strength of concrete,  ${}_J \delta_c$ : coefficient on joint type (=3: interior beam-column joint,

=2: exterior beam-column joint),  $a_e$ : effective area of concrete panel ( $=b_e \times d_e$ ),  $b_e$ : effective width of concrete panel (average of column-width, and beam-width),  $d_e$ : effective depth of concrete panel (the distances between center of steel flange),  $\sigma_y$ : yield stress of steel panel web,  $A_{sw}$ : section of steel panel web,  $l$ : span of beam,  $h$ : span of column,  $j_b$ : effective depth of beam,  $j_c$ : effective depth of column.  $j_b$  and  $j_c$  are the distances between center of steel flange of beam and column, respectively.

The specimens were loaded with lateral cyclic shear forces by a horizontal hydraulic jack. Interior beam-column joints were subjected to constant axial compression of 775 kN, of which the axial force ratio ( $N / (b \cdot D \cdot \sigma_B)$ ) is 0.15. And exterior beam-column joints were subjected to varying axial force given by Eqn. (4) using two vertical hydraulics jacks. The incremental loading cycles were controlled by story drift angles,  $R$ , defined as the ratio of lateral displacements to the column height,  $\delta/h$ .

$$N = 0.1 b \cdot D \cdot \sigma_B \pm 3Q \quad (4)$$

Where,  $N$ : axial force,  $b$ : width of column,  $D$ : depth of column,  $\sigma_B$ : compressive strength of concrete,  $Q$ : lateral force, respectively.

### 3. THREE-DIMENSIONAL NON-LINEAR FEM ANALYSIS

#### 3.1 Analytical Model

A three-dimensional non-linear FEM analysis was conducted to investigate the stress transferring mechanism of the joint panel region of the CES beam-column joints, using the non-linear FEM analysis software "FINAL" [2]. The finite element model used was calibrated against experimental results. The analytical model was a half model considering the symmetry of the specimens. The finite element mesh layout for the CES beam-column joints is shown in Fig. 3. The bottom end of the column had a pin support, and the ends of beams had roller supports to restrain vertical displacement. The top of the column was subjected to lateral displacement reversals with a constant axial load of 387.5kN ( $=775/2$ kN) in Specimens CESJ-A and CESJ-B. Axial loads measured in the experiments were applied for Specimens CESJ-AE and CESJ-BE subjected to varying axial loads, (CESJ-AE: -67~713 kN, CESJ-BE: -263~1,050 kN).

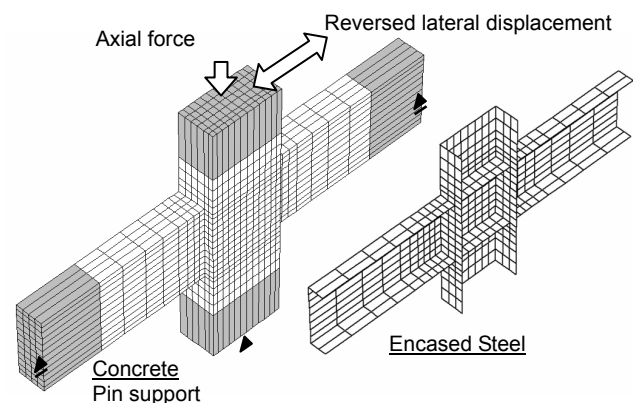


Figure 3 Finite element mesh (CESJ-A)

#### 3.2 Element Model

The quadrilateral plane stress element was used for steel web. Steel flanges were modeled by the shell elements, in which shear deformation and bending deformation in out-of-plane are considered. The material model of steel plates was a plasticity model, which was the Von Mises' failure surface with the associated plastic rule. The stress-strain curve of steel was idealized by a bi-linear model, and the isotropic hardening rule was adopted as the hysterical model. Encased steel was connected to the pin supports at the ends of the beams and columns that were idealized by the eight node hexahedral element of steel. Mechanical properties of steel model in the analysis used are shown in Table 2.

Mechanical properties of concrete model in the analysis used are shown in Table 3. FRC elements were modeled by the eight node hexahedral element with three global degrees of freedom per node. As for the stress-strain relationship of FRC, a modified Ahmad model [3] was adopted for the compressive stress-strain curve in the stress-rising regions; the compressive stress-strain curve in the stress-softening regions was modeled by a multi-linear model using substantial data from material tests shown in Fig. 5(a). The five-parameter model of Willam-Warnke [3] was adopted as the fracture criterion of concrete, and the

Table 2 Mechanical properties of steel model used in the analysis

	Yielding stress (MPa)	Elastic modulus (GPa)	site	Specimen
H-300×220 ×10×15	284.0	190	flange	CESJ-A
	295.5		Web	CESJ-B
PL - 4.5	256.7		Panel	CESJ-B
H-300×150 ×6.5×9	320.5		flange	CESJ-A
	407.7		web	
H-300×200 ×9×19	251.6		flange	CESJ-B
	293.1		web	
H-300×220 ×10×15	304.2		flange	CESJ-AE
	318.9		web	CESJ-BE
PL - 4.5	306.9		panel	CESJ-BE
H-300×150 ×6.5×9	304.0		flange	CESJ-AE
	348.4		web	
H-300×200 ×9×19	281.1		flange	CESJ-BE
	304.3		web	

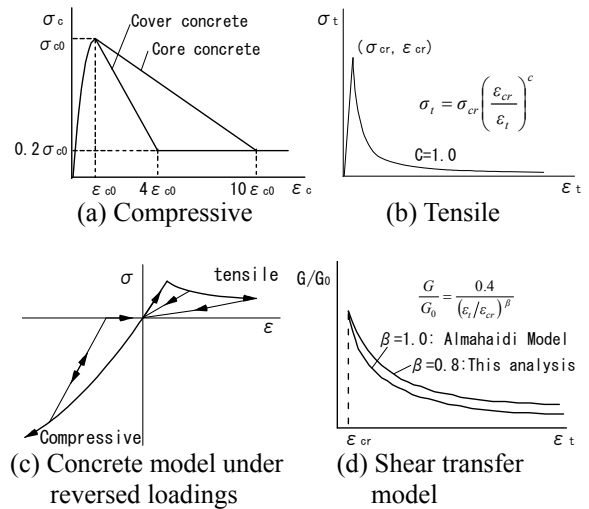


Figure 5 Constitutive laws for concrete

Table 3 Mechanical properties of concrete model used in the analysis

	$\sigma_c$ (MPa)	Ft (MPa)	Ec (GPa)		$\epsilon_{c0}$ ( $\mu$ )	
			Ana	Test	Ana	Test
CESJ-A	33.3	1.90	20.2*	—	2500	—
CESJ-B	31.6	1.85	24.8	—	2500	—
CESJ-AE	40.0	2.08	21.9*	29.8	2500	2464
CESJ-BE	38.0	2.04	21.4*		2500	

$\sigma_c$  : compressive strength of concrete, Ft : stress of concrete at crack,  $Ft=0.33\sqrt{\sigma_c}$ , Ec : elastic modulus calculated by AIJ standard (\* decreased to 80%),  $\epsilon_{c0}$  : Strain at compressive strength

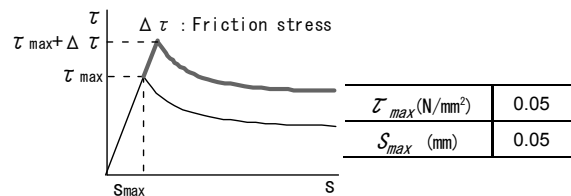


Figure 6 Relationship of bond stress and slip between steel and concrete

compressive strength reduction factor was adopted from Vecchio and Collins [4]. Tension stress was taken to be very small after the crack occurred, and the concrete tension model by Izumo [5] with coefficient, c of 1.0, was used in the descending branch (Fig. 5(b)). Stiffness reduction due to cyclic stress was not considered (Fig. 5(c)). The Al-mahaidi model [3] was used as the shear transfer model after cracks occurred in the concrete element. Where, in Al-mahaidi model,  $\beta$  of 1.0 was changed to  $\beta$  of 0.8 to decrease shear transfer stiffness (Fig. 5(d)), so strength deterioration and stiffness reduction in the analytical results tend to be larger than test results. It is thought that this behavior is due to the follows reasons; because CES structure system does not have reinforcement bars, the damage to concrete is little due to the dowel action in reinforced concrete.

The film element was used as the bond model between concrete and steel. Bond stresses in the bond stress-slip relationship at the interface between concrete and steel were assumed to be  $0.05\text{N/mm}^2$ , and concrete was assumed to be under low confined stress. Meanwhile, friction stress caused by compressive stress was considered with friction coefficients of 0.65 (Fig. 6).

### 3.3 Comparison Analysis with Test

Figure 7 shows comparisons between experimental and analytical results on the columns shear versus drift angle relationships for all specimens. For Specimen CESJ-A, although the initial stiffness in the analytical results tend to be larger than those in the experimental results, the analytical backbone curve agrees well with the experimental one until a drift angle, R, of 0.03 rad. The maximum shear force in the analysis is 539kN, which is almost the same as the experimental value, 517kN. The initial stiffness in the analysis for Specimen CESJ-B is also evaluated to be larger than the experimental results, while the backbone curve by the analysis

shows good agreement with the experimental one. The maximum shear force in the analysis is 551kN, which is almost the same as the experimental value of 564kN, and the corresponding drift angle is 0.015 rad. As for Specimens CESJ-AE and CESJ-BE which are exterior joints, although the initial stiffnesses and the maximum shear forces in the analysis are larger than experimental results in the negative loading that tensile axial force applied to the specimens, the backbone curves of analysis are good agreement with experimental ones in the positive loading.

The shear deformations in shear panel for Specimen CESJ-B, which showed significant joint shear failure, and Specimen CESJ-BE are shown in Fig. 8. Each deformation in both analysis and experiment is calculated based on the measured displacement of steel shown in Fig. 8. Analytical shear deformation for specimen CESJ-B is good agreement with experimental one. The results of Specimen CESJ-A show the same tendency as that of Specimen CESJ-B. Analytical shear deformation for Specimen CESJ-BE that was applied varying axial force is smaller than the experimental result. Shear stress versus shear strain relationship calculated by rosette analysis with measured strain at center of web panel and analytical result of steel element corresponding to them are shown in Fig. 9. Absolute values of shear stresses at the each peak are plotted until drift angle of 0.02 rad.. The analytical shear strain of the joint panel for Specimens CESJ-B and CESJ-BE sufficiently simulated the behavior of the experimental results.

In general, the backbone curve and deformation of joint panel agree well with experimental results, and it is confirmed that this analytical model can mostly simulate behavior of CES beam-column joint.

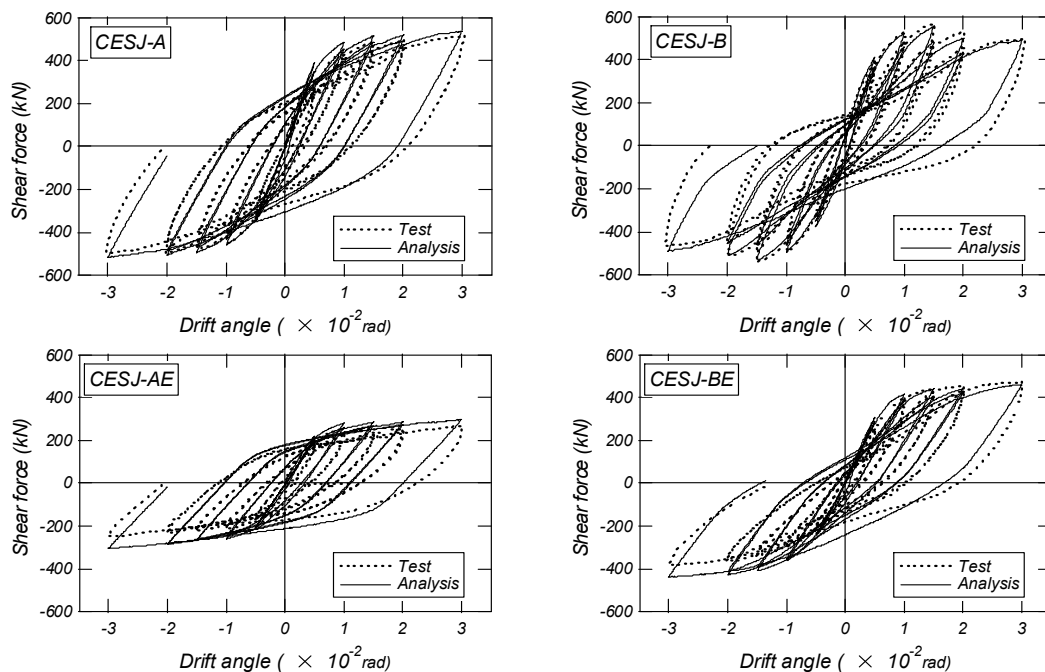


Figure 7 Shear force - drift angle relationships

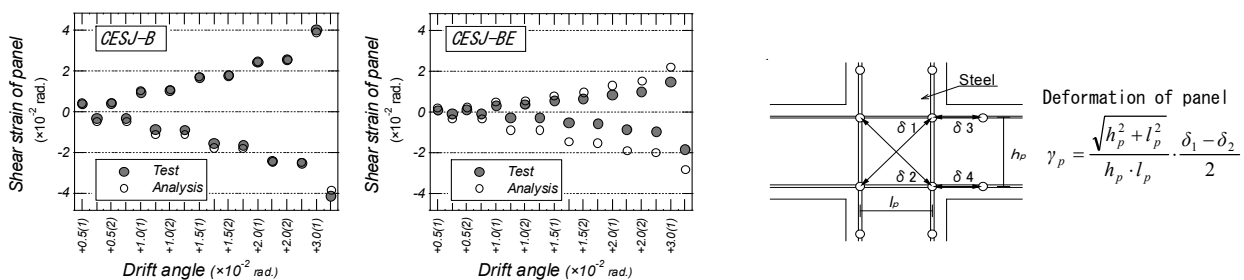


Figure 8 Shear deformation of joint panel

#### 4. STRESS STATE IN THE JOINT PANEL

The validity of material constitutive law and analytical assumptions used may be confirmed through comparisons between experimental and analytical results on the shear versus drift angle relationships and the shear deformation of joint panel, as shown in the previous section. Then, the inner stress state of joint panel is discussed using analytical results in this section.

Figure 10 shows the principal compressive stress of concrete in the joint of Specimens CESJ-B and CESJ-BE of which the shear capacity magnification factors are small. The positions of these elements are shown in Fig. 12. For Specimen CESJ-BE subjected to varying axial force, the results in both positive and negative loadings are shown in Fig. 10. It can be seen that the resultant compressive strut of concrete was formed in the element C2 where an inner panel region surrounded by the steel flange of the beam and column. High stresses over the compressive strength of concrete also occur at the corner of inner concrete. Compressive stresses in the element C4 and C6 that the confined effect would be small due to the absence of the steel flange are smaller than that of the element C2. However, the compressive stress field is larger than that in the element C2. For Specimen CESJ-BE subjected to varying axial forces, the width of the compressive strut formed in region surrounded by the steel flange under tensile axial force in the negative loading is narrower than that under compressive axial force in positive loading, and the stress level is generally small. Thus, it is confirmed that the inner stress state is different depending on the applied axial force level.

Figure 13 shows the shear force distribution in the horizontal cross-section at the central height of the joint panel of Specimens CESJ-B and CESJ-BE. The positions of referring concrete and steel elements to the shear forces contributed are shown in Figs. 11 and 12. As for Specimen CESJ-B, the shear force contributed by concrete makes up most of total shear force. In addition, it is confirmed that concrete elements C4

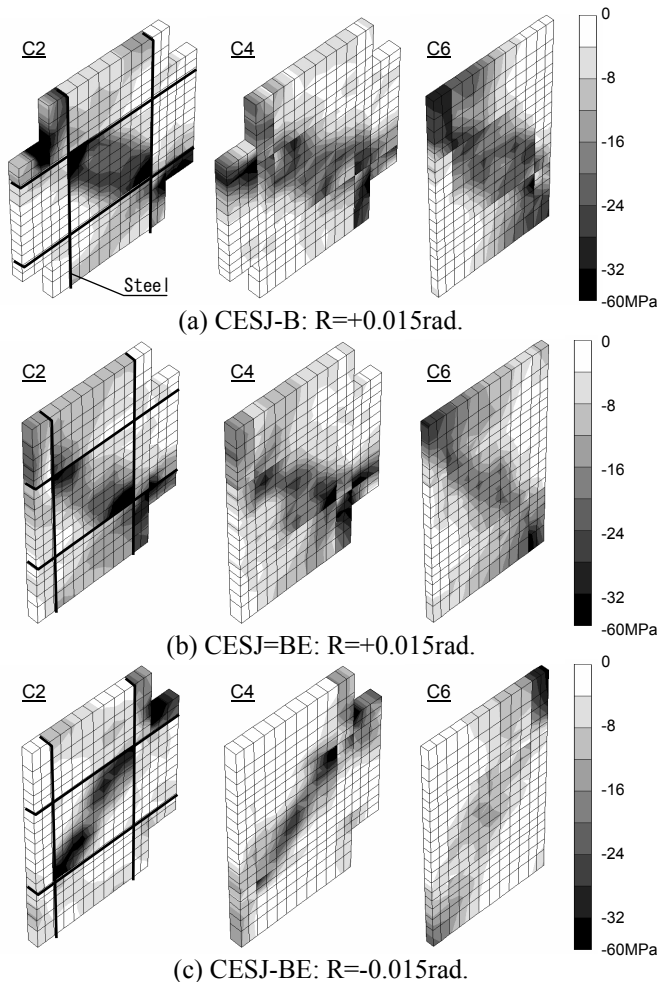


Figure 10 Principal compressive stress of joint

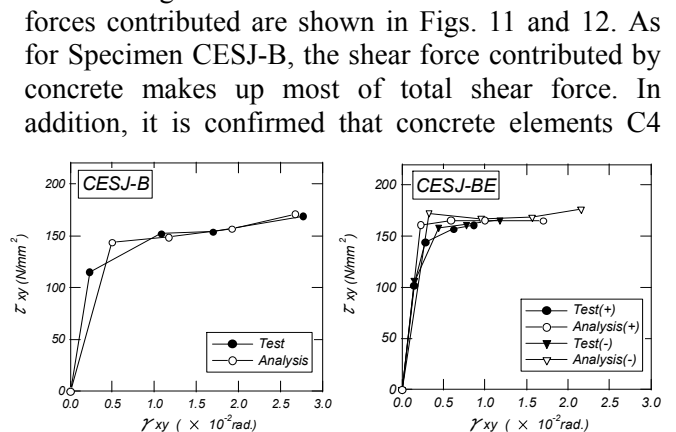


Figure 9 Shear stress - shear strain relationship of element in web panel

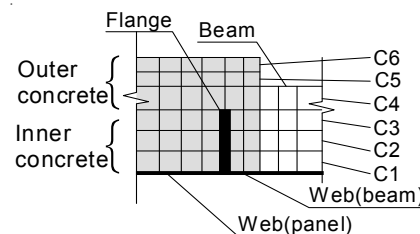


Figure 11 Position and name of elements

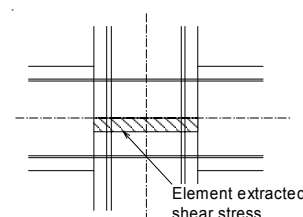


Figure 12 Position of referring element to shear stress

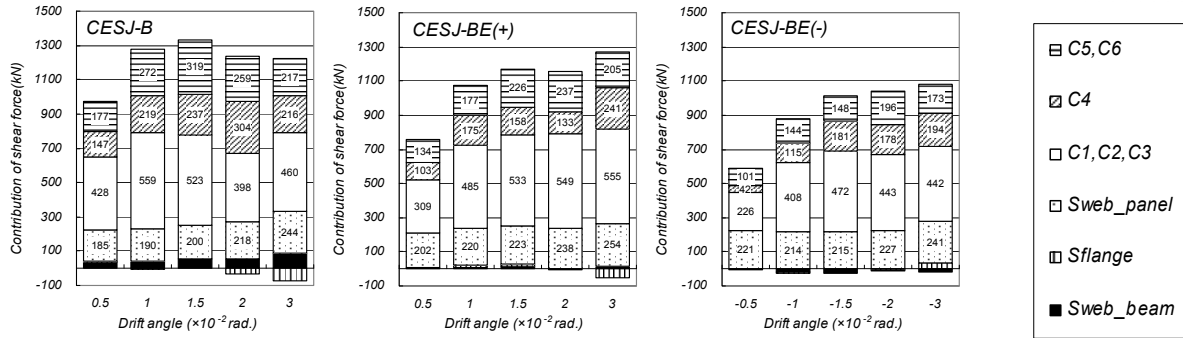


Figure 13 Shear force distributions of joint panel

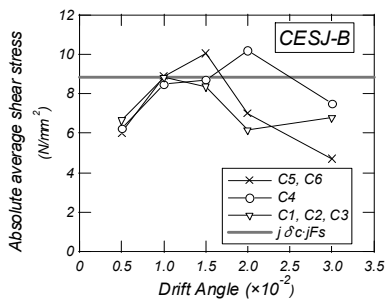


Figure 14 Shear stress contributed by concrete of joint panel (CESJ-B)

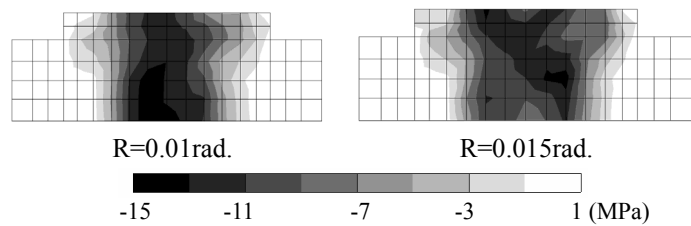


Figure 15 Distribution of shear stress of concrete of joint panel (CESJ-B)

through C6 that are not surrounded with the steel flange also share the same shear force as elements surrounded with the steel flange. This corresponds to results that wide compressive stress field is formed in outer concrete as shown in Fig. 10. It is also found that the steel webs in beams, which is adjacent to the joint panel region, slightly contribute shear forces and act as a part of joint panel. Comparing shear force at the positive loading with that at negative loading in Specimen CESJ-BE, although the shear forces contributed by steel are not different so much, the shear forces contributed by concrete at negative loading with tensile axial force are smaller than that at positive loading. It is found that the axial force level affects the stress state of concrete panel in these specimens.

For concrete elements of joint panel of Specimen CESJ-B that showed a significant joint shear failure, the average shear stresses at peak in each positive loading cycle are shown in Fig. 14. In the figure, the value of  $(j \delta_c \cdot j F_c)$  in Eqn. (2), which is multiplied shear strength of concrete by coefficient on joint type, is also shown. The position of referring elements to shear stresses contributed by concrete are shown in Fig. 11. It is found that shear stresses in both inner and outer concrete regions reach the stress corresponding to  $(j \delta_c \cdot j F_c)$  at drift angle of 0.01rad.. Shear stresses in the outer concrete region rise with increasing drift angle until 0.015 rad., while shear stresses in the inner concrete region keep up the stress corresponding to  $(j \delta_c \cdot j F_c)$ . It is also found that transition of the shear stress between inner and outer concrete regions are different. Namely, because the shear distortion in the outer concrete region develops to follow that in the inner one, and regions of concrete developing shear stresses extend toward the outside as shown Fig. 15, which is shear stress contours in concrete elements. It is confirmed that shear force developing in joint panel is sustained in larger area than effective area described in Eqn. (2).

## 5. SHEAR STRENGTH EVALUATION OF CES JOINTS

Calculated strengths of columns, beams, and a joint panel for each specimen are listed in Table 4 with the measured maximum shear forces. The calculation was executed by using method described in Section 2. In the calculation of the joint shear strength, two effective concrete areas, the effective areas (a) and (b) are assumed as shown in Fig. 17. Specimen CESJ-A and CESJ-AE, whose calculated ultimate flexural strength of beam is smaller than the calculated strengths of the column and joint panel, is evaluated as a beam flexural failure. This

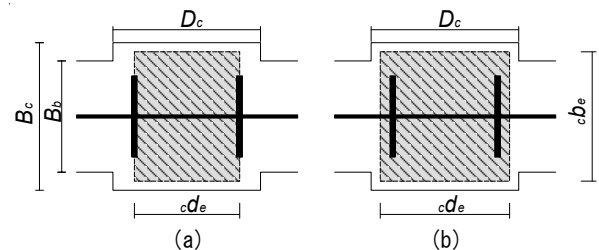
Table 4 Measured and calculated ultimate strength

Specimen	Calculation			Test	
	Flexural strength of beam	Flexural strength of column	Joint shear strength		Maximum shear force
			panel(a)	Panel(b)	
CESJ-A	466	1123	511	-	517
CESJ-B	716	1117	364	499	564
CESJ-AE	214	1358 (-924)	436	-	270 (-264)
CESJ-BE	394	1447 (-800)	302	-	473 (-383)

Corresponding value to shear force of column

Unit: kN

corresponds to failure mode in the experimental results. Specimen CESJ-B, whose calculated ultimate shear strength of joint panel is smaller than the calculated strengths of the column and beam, is evaluated as the joint shear failure. This also corresponds to the experimental results. However, since the ratio of the measured maximum shear force to the calculated one using the effective area (a) is 0.65 for Specimen CESJ-B, it seems that the assumption of the effective area (a) gives underestimation of the joint shear strength. When using the effective area (b), on the other hand, the ratio is 0.89 and the evaluation accuracy is improved.



(a):  $cd_e$  = the distances between center of steel flange  
(b):  $cb_e$  = Average of column depth and steel flange depth

Figure 17 Effective area assumed

## 6. CONCLUSIONS

Non-linear FEM analyses of beam-column joints for composite CES structural systems consisting of steel and fiber reinforced concrete were conducted to examine the stress transferring mechanism of the joints, together with verifying applicability of the analysis method. The following conclusions can be drawn.

- 1) The analytical results show good agreement with the experimental ones on the story shear versus story drift relationship for CES beam-column joints. Namely it is thought that the analytical method used seems to be almost valid for simulating the behavior of CES beam-column joints.
- 2) It is confirmed that the compressive concrete strut was formed in the outer concrete panel region as well as in the inner concrete panel region surrounded by the steel flange of the beam and column. It is also found that analyzed shear forces in the outer panel are contributed almost the same level as those in the inner panel at the maximum capacity of the beam-column joint.
- 3) Applied axial force level affects the stress transferring condition of the compressive concrete strut developed in the joint panel.
- 4) Joint shear strength of interior CES beam-column joints could be evaluated by a method based on the AIJ design standard for SRC structures modifying effective area of concrete and steel. However, more detailed investigation is necessary, because of this results are of limited specimens.

## REFERENCES

- [1] Architectural Institute of Japan. (2001). AIJ Standard for Structural Calculation of Steel Reinforced concrete Structure (in Japanese)
- [2] "FINAL/99". ITOCHU Techno-Solutions Corporation
- [3] K Naganuma. (1995). Stress-strain relationship for concrete under triaxial compression. Journal of structural and construction engineering. No.474. 163-170. (in Japanese)
- [4] Vecchio,F.J. and Collins,M.P. (1986). The Modified Compression-Field Theory for Reinforced Concrete Elements Subjected to Shear. ACI Journal. Vol.83. No.2. 219-231
- [5] J Izumo. (1989). Analysis model for a reinforced concrete panel element subjected to reversed cyclic in-plane stress. Journal of structural mechanics and earthquake engineering. No.408. 51-60. (in Japanese)